

## SELF-ALIGNED MICRO BUBBLE ARRAYS BY USING SURFACE TENSION

De-Sheng Meng\* and Chang-Jin "CJ" Kim  
Mechanical and Aerospace Engineering Department,  
University of California, Los Angeles  
Los Angeles, CA 90095, U.S.A.

### ABSTRACT

This paper describes the theory and experiments involve in the capture of bubbles onto a patterned surface. Guided by surface free energy, bubbles can automatically attach to the energetically favorable locations (bubble-traps) and align into bubble arrays. Bubble capturing potential  $F_{bc}$  is proposed as the quantity to evaluate the surface's "affinity" for bubbles. A bubble-trap can therefore be viewed as an area with locally maximum positive  $F_{bc}$ . Two types of bubble-traps are proposed and evaluated. Type I bubble-traps are hydrophobic patterns on a hydrophilic flat surface. Type II bubble-traps are concave conic pits surrounded by a hydrophilic flat surface. Simulation of bubble capturing potential  $F_{bc}$  explains the bubble-capturing behavior for both cases and predicts a better performance for type II bubble-traps. Experiments agree well with the theoretical prediction and suggest promising applications.

### INTRODUCTION

Microscopic gas bubbles can be of great interest for both scientific research and engineering applications. They can serve as pressure sensors [1], imaging particles [2], signal sources for MRI (Magnetic Resonance Imaging) [3] and microlenses. Agitated by acoustic waves, microscopic gas bubbles are known to emit ultrashort flashes of light (a phenomenon named sonoluminescence) [4], and support an environment with extreme conditions inside [5]. However, reliable manipulation of these bubbles is necessary so that their remarkable properties can be employed to perform specific tasks consistently. Trapping bubbles onto pre-determined locations (e.g. arrays) is one of the basic manipulations. Hydrophobic microwells were reported to be able to capture bubbles by using surface tension [6], the dominant force in sub millimeter dimensions [7]. But quantitative analysis of the bubble capturing structure (i.e. bubble-traps) is still absent. This paper proposes bubble capturing potential ( $F_{bc}$ ) as the quantity to evaluate a bubble-

trap's potential to capture a gas bubble onto it from a liquid environment, so as to provide a design guideline for relevant microfluidic devices.

### KEYWORDS

Bubble-trap; Bubble array; Bubble capturing potential; Surface free energy.

### BUBBLE-TRAPS: QUALITATIVE EXPLANATION

The bubble capturing mechanism is based on the multiphase fluidic system's tendency to minimize its total surface energy. If a pattern on heterogeneous surface provides lower total energy for a bubble on it than its vicinity does, this pattern is called a bubble-trap. When a bubble gets a chance to move around, it will tend to stay on a bubble-trap so that the total system energy is minimized. The energy here is surface free energy, whose components can be found in Young's equation of contact angle (figure 1):

$$g_{vl} \cos q = g_{sv} - g_{sl} \quad (1)$$

where  $g_{vl}$ ,  $g_{sv}$  and  $g_{sl}$  are the surface free energy of liquid-vapor, solid-vapor and solid-liquid interfaces respectively, and  $q$  is contact angle.

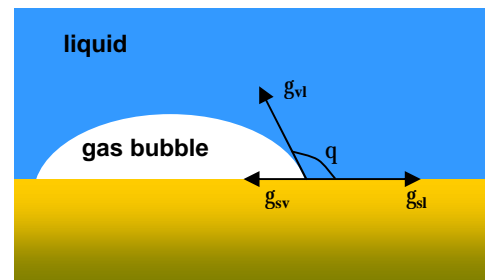


Figure 1. Contact angle of a three-phase interface

\* Submitting author, Email: [desheng@seas.ucla.edu](mailto:desheng@seas.ucla.edu)

The total surface energy of the system can then be defined as:

$$E = \sum A \cdot \mathbf{g} = A_{vl} \cdot \mathbf{g}_{vl} + A_{sv} \cdot \mathbf{g}_{sv} + A_{sl} \mathbf{g}_{sl} \quad (2)$$

where  $A_{vl}$ ,  $A_{sv}$  and  $A_{sl}$  are the surface areas of liquid-vapor, solid-vapor and solid-liquid interfaces respectively. Bubble-trap is a location where total surface energy is minimized when a bubble is attached onto it. Figure 2 is a schematic drawing of the two kinds of proposed bubble-traps.

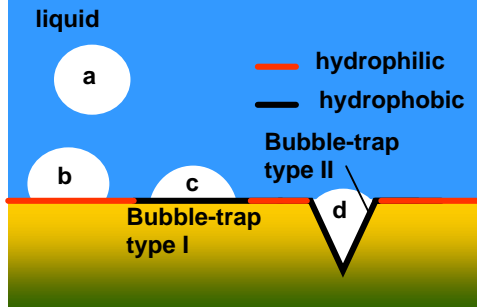


**Figure 2.** Bubbles' status in three-phase system  
a: floating; b, c and d: attached

Type I bubble-trap is a hydrophobic pattern on a flat hydrophilic surface. To simplify the argument but still understand bubble capturing qualitatively, we assume the liquid-vapor surface is kept constant whether a floating bubble (bubble "a" in figure 2) attaches to a hydrophilic flat surface (bubble "b") or hydrophobic flat surface (bubble "c"). Then the bubble attachment process can be viewed as substituting a solid-liquid interface with area  $DA$  by a solid-vapor interface with the same area, resulting in an increase of system energy by  $DE = DA(\mathbf{g}_{sv} - \mathbf{g}_{sl})$ . When  $\mathbf{q}$  is smaller than  $90^\circ$  (hydrophilic), or  $\mathbf{g}_{sv} > \mathbf{g}_{sl}$ ,  $DE > 0$ , i.e. the formation of a solid-vapor interface increases the system energy. This is not favorable, so the bubbles tend to detach from the hydrophilic surface. Vice versa, when  $\mathbf{q}$  is larger than  $90^\circ$  (hydrophobic), or  $\mathbf{g}_{sv} < \mathbf{g}_{sl}$ ,  $DE < 0$ , i.e. the formation of a solid-vapor interface decreases the system energy. This is favorable, so the bubbles tend to attach to the hydrophobic surface. This somewhat oversimplified model explains why a hydrophobic spot on a hydrophilic surface can serve as a bubble-trap to capture the bubbles from a liquid environment and hold them.

A hydrophobic concave pit on a hydrophilic surface can serve as an even better bubble-trap (type II). Two factors contribute to this geometrically enhanced bubble-trap. First, a larger interface ( $DA$ ) is "exchanged" during bubble capturing (bubble d of figure 2), compared with a flat surface. This larger area  $DA$  entails a larger energy reduction in  $DE = DA(\mathbf{g}_{sv} - \mathbf{g}_{sl})$  and promotes the capturing. Second, the liquid-vapor interface of a bubble can also be reduced significantly in the attaching process, and thus is the total energy.

### BUBBLE CAPTURING POTENTIAL $F_{BC}$

The qualitative explanation above can help understand the bubble capturing phenomenon. But it is not accurate, because the bubbles will deform during this attach-detach process, so the liquid-vapor surface area is also changing. Moreover, the total energy in equation 2 depends on the bubble size and

absolute value of liquid surface tension, so it cannot be used as an indicator for the bubble-trap's bubble capturing ability.

In order to eliminate the influence of bubble size and liquid properties, the scale to evaluate the surface's "affinity" for gas bubbles is defined as bubble capturing potential:

$$\Phi_{bc} = -(E - E_0) / L^2 \cdot \mathbf{g}_{vl} \quad (3)$$

where  $E_0$  is the total surface energy of a three-phase system with a floating bubble (i.e. bubble a in figure 2);  $E$  is the total surface energy of a three-phase system with an attached bubble (bubble b, c or d in figure 2);  $L = V^{1/3}$  stands for the characteristic length of the bubble; and  $\mathbf{g}_{vl}$  stands for the surface free energy on vapor-liquid interface.

According to the definition, a surface with positive  $F_{bc}$  means system energy will decrease during bubble detaching, which is energetically favorable. So a bubble tends to be captured on a surface with positive  $F_{bc}$ . An area with larger  $F_{bc}$  represents a stronger tendency to retain bubbles on it. A bubble-trap can therefore be viewed as an area with locally maximum (and positive)  $F_{bc}$ .

Here, we assume the patterns or pits are big enough to accommodate the bubbles. Or conversely, the bubble is small enough to be accommodated in a single bubble-trap. In this case, we will show that  $F_{bc}$  only depends on surface topology and contact angle in the following deduction.

The volume of the floating bubble (bubble a) is  $V = \frac{4}{3} \mathbf{p} \cdot R^3$ . So the characteristic length of this bubble is  $L = \sqrt[3]{V} = \sqrt[3]{\frac{4}{3} \mathbf{p} \cdot R^3}$ . Therefore the surface area (vapor-liquid interface) is:  $A_{vl}^0 = 4 \mathbf{p} \cdot R^2 = \sqrt[3]{36 \mathbf{p}} \cdot L^2$ .

Therefore, the introduction of a floating bubble into the three-phase system leads to a total surface energy increase of:

$$E_0 = A_{vl}^0 \cdot \mathbf{g}_{vl} = \sqrt[3]{36 \mathbf{p}} \cdot L^2 \cdot \mathbf{g}_{vl} \quad (4)$$

However, the introduction of an attached bubble into the three-phase system causes two area changes. Firstly, a surface area is dried, or a solid-liquid interface is replaced by a solid-vapor interface. Secondly, the area of vapor-liquid interface is changed. The total surface energy of an attached bubble is hence:

$$E = A_{vl} \cdot \mathbf{g}_{vl} + A_{dry} \cdot \mathbf{g}_{sv} - A_{dry} \cdot \mathbf{g}_{sl} \quad (5)$$

Since  $\mathbf{g}_{sv} - \mathbf{g}_{sl} = \mathbf{g}_{vl} \cdot \cos \mathbf{q}$  (equation 1), equation 5 becomes:

$$E = (A_{vl} + A_{dry} \cdot \cos \mathbf{q}) \cdot \mathbf{g}_{vl} \quad (6)$$

Substitute (4) and (6) into equation 3, the bubble capturing potential:

$$\begin{aligned} \Phi_{bc}(\mathbf{q}) &= \sqrt[3]{36 \mathbf{p}} - \frac{A_{vl}}{L^2} - \frac{A_{dry}}{L^2} \cos \mathbf{q} \\ &= \sqrt[3]{36 \mathbf{p}} - \underline{A}_{vl} - \underline{A}_{dry} \cos \mathbf{q} \end{aligned} \quad (7)$$

where  $A_{vl}$  and  $A_{dry}$  stand for vapor/liquid and vapor/solid interface area of the attached bubble respectively. They are typically proportional to  $L^2$ , if the particular pattern can accommodate the bubble completely (i.e. bubble is small enough). The corresponding normalized area  $\underline{A}_{vl}$  and  $\underline{A}_{dry}$  are functions of surface topology and contact angle only. Consequently,  $F_{bc}$  is independent of the absolute value of surface tension and bubble size. Elimination of these two variables makes  $F_{bc}$  valid for a particular bubble with any size in a specified liquid with any  $g_{vl}$  value. In other words,  $F_{bc}$  is a mere property of the surface for a given contact angle.

If a big bubble attaches onto an area including two or more patterns, the bubble capturing potential will be the weighted average  $F_{bc}$  of all the patterns that it touches. However,  $F_{bc}$  is more meaningful for microscopic gas bubbles, because surface tension of large bubble is less significant and can be neglected in a lot of circumstance.

### BUBBLE-TRAPS: QUANTITATIVE ANALYSIS

Equation 7 provided the foundation to calculate bubble capturing potential of any surface structure, including bubble-traps, a surface area with locally maximum (and positive)  $F_{bc}$ . Bubble capturing potential of flat surface and the concave conic pit will be analyzed to evaluate the two kinds of bubble-traps mentioned before.

On a flat surface as figure 3 represents, the height of a attached bubble is:  $h = (1 + \cos q) \cdot R$ .

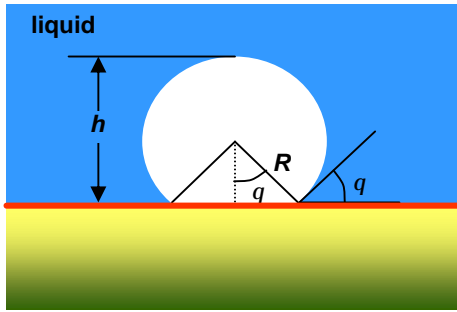


Figure 3. A gas bubble on flat surface

So the relationship between characteristic length  $L$  and radius  $R$  of this attached bubble can be calculated by means of its volume:

$$\begin{aligned} L^3 = V &= \frac{\rho}{3} \cdot h^2 \cdot (3R - h) \\ &= \frac{\rho}{3} (1 + \cos q)^2 \cdot (2 - \cos q) \cdot R^3 \end{aligned} \quad (8)$$

Then the vapor-liquid interface area  $A_{vl}$  and vapor-solid interface area  $A_{dry}$  can be expressed by characteristic length  $L$ .

$$A_{vl} = 2\rho R h = \underline{A}_{vl}(q) \cdot L^2 \quad (9)$$

$$A_{dry} = 2\rho (R \sin q)^2 = \underline{A}_{dry}(q) \cdot L^2 \quad (10)$$

Both  $\underline{A}_{vl}(q)$  and  $\underline{A}_{dry}(q)$  here are mere functions of contact angle  $q$ , which means that  $F_{bc}$  on flat surface is a mere function of contact angle.

Similar calculations can be applied to concave conic pits, as figure 4 illustrates.

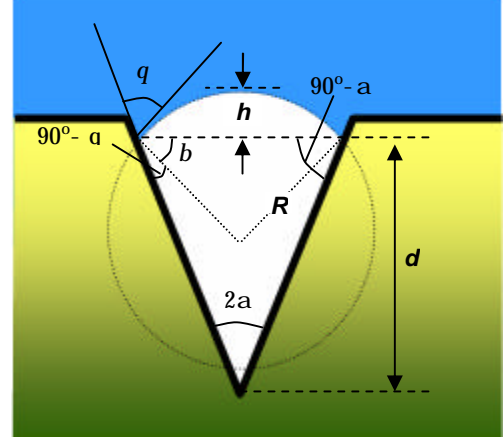


Figure 4. A gas bubble in a concave conic pit

The angle between the radius of bubble meniscus and horizontal level is:

$$b = q - a \quad (11)$$

where  $a$  stands for the conic angle of the pit and  $q$  stands for the contact angle.

Knowing this angle, the volume of upper spherical cap can be calculated as:

$$V_s = \frac{\rho}{3} \cdot h^2 \cdot (3R - h) \quad (12)$$

where,  $h = (1 - \sin b) \cdot R$  is the height of the cap. What need to be noticed is that this volume  $V_s$  should be considered negative when  $b > 90^\circ$  and the spherical cap is concave (refer to figure 5). We can rewrite equation 12 as:

$$V_s = \frac{\rho}{3} \cdot h^2 \cdot (3R - h) \cdot \text{sign}(\cos b) \quad (13)$$

The sign function here is defined as:

$$\text{sign}(x) = \begin{cases} 1, & \text{if } x > 0 \\ 0, & \text{if } x = 0 \\ -1, & \text{if } x < 0 \end{cases} \quad (14)$$

The volume of the dry part of this conic pit is:

$$V_c = \frac{\rho}{3} \cdot r^2 \cdot d \quad (15)$$

where the radius of the cone bottom is  $r = R \cdot |\cos b|$  and the depth of the conic pit is  $d = r / \tan a$ .

Then we can get the relationship between  $R$  and  $L$  as:

$$L^3 = V = V_s + V_c = \underline{V}(q, a) \cdot R^3 \quad (16)$$

$\underline{V}(q, a)$  here is a dimensionless parameter, determined by equation 13-16. It is a function of contact angle  $q$  and conic angle  $a$ .

Then the vapor-liquid interface area  $A_{vl}$  and vapor-solid interface area  $A_{dry}$  can be expressed by characteristic length  $L$ .

$$A_{vl} = 2pRh = \underline{A}_{vl}(\mathbf{q}, \mathbf{a}) \cdot L^2 \quad (17)$$

$$A_{dry} = 2pr \cdot \sqrt{d^2 + r^2} = \underline{A}_{dry}(\mathbf{q}, \mathbf{a}) \cdot L^2 \quad (10)$$

Again, both  $\underline{A}_{vl}(\mathbf{q}, \alpha)$  and  $\underline{A}_{dry}(\mathbf{q}, \alpha)$  here are mere functions of contact angle  $\mathbf{q}$  and conic angle  $\alpha$ , which means that  $F_{bc}$  of

concave conic pits is a function of contact angle and conic angle.

Figure 5 shows the change of bubble shape according to variable contact angle and its effect on the sign of volume and surface area.

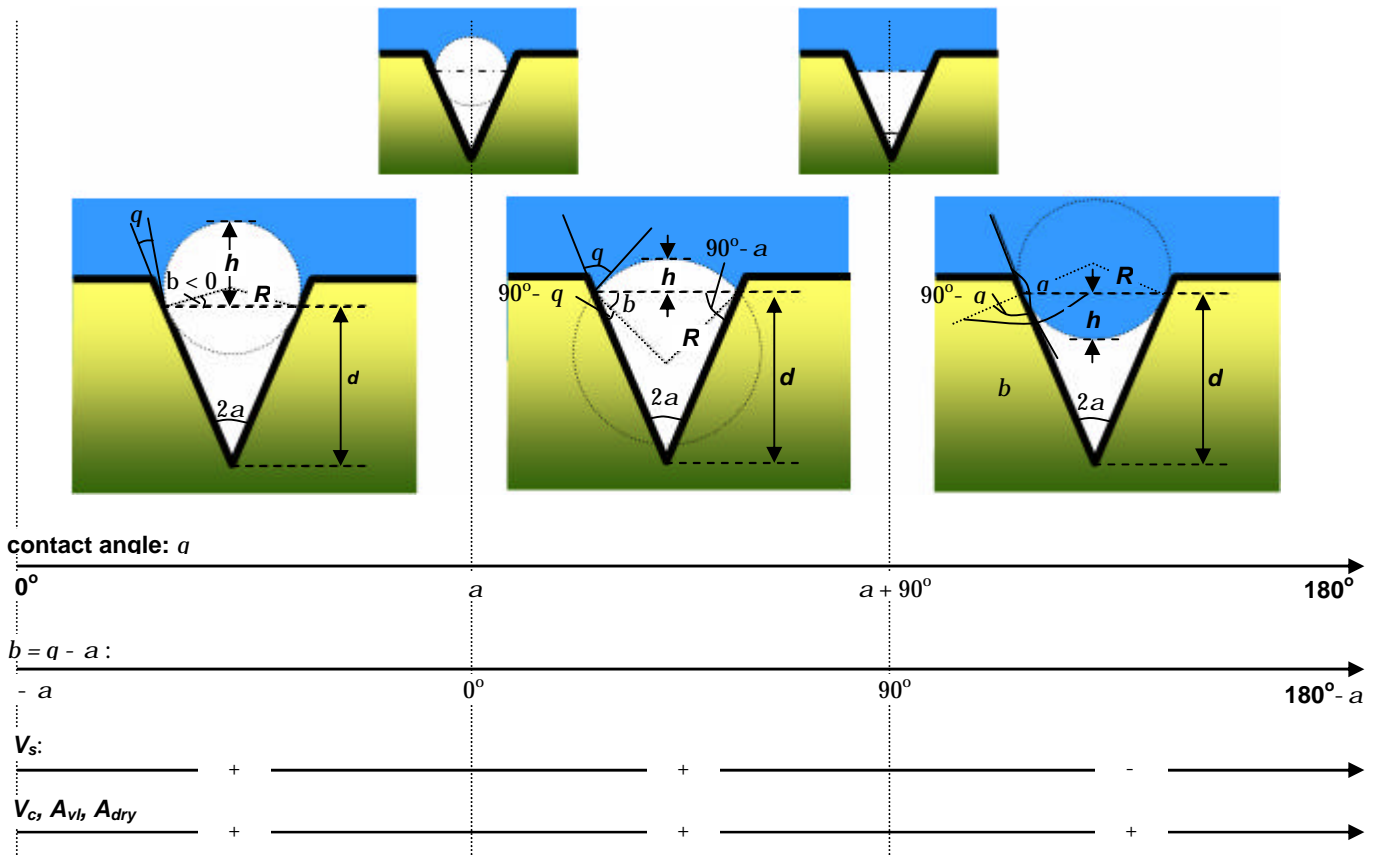


Figure 5. bubble shape for different contact angle

## SIMULATION RESULTS

Matlab<sup>®</sup> simulation results of flat surface and conic pit are shown in figure 6, assuming a contact angle range of  $0^\circ$  to  $180^\circ$ . The conic angle is set to  $40^\circ$  to represent KOH-etched silicon pits, which have a maximum tilt angle of  $45^\circ$  and a minimum tilt angle of  $35^\circ$ . KOH-etching is the most convenient way to get relatively hydrophobic concave pits. This is also the reason why KOH-etched pits are used as the bubble-trap in our application example, to be mentioned later in this paper.

Two interesting aspects can be found in these curves: Firstly, a surface doesn't need to be strictly hydrophobic in order to capture bubbles. For both the flat surface and conic pit,  $F_{bc}$  turn positive at contact angle value as small as  $\sim 20^\circ$ . Accordingly, given a contact angle larger than  $20^\circ$ , even attaching onto a hydrophilic surface can be more energetically favorable than floating in the liquid for a bubble. This can be confirmed by the observation that bubbles can form on the wall of a water-filled glass beaker (contact angle around  $20^\circ$ ) and stay there, when the beaker is heated. However  $F_{bc}$  increases dramatically with increasing contact angle after it is larger than  $\sim 80^\circ$ . Secondly, the simulation results suggest a substantially higher  $F_{bc}$  for the concave structures, compared to a flat surface

with the same contact angle for most of the range of  $q$  (i.e.  $q > 20^\circ$ ). This predicts a stronger bubble attraction of the Type II bubble-traps. For example,  $F_{bc}$  of a conic pit at  $80^\circ$  contact angle is 1.91 - almost 3 times that of  $F_{bc}$  for the flat surface (0.69) with the same contact angle.

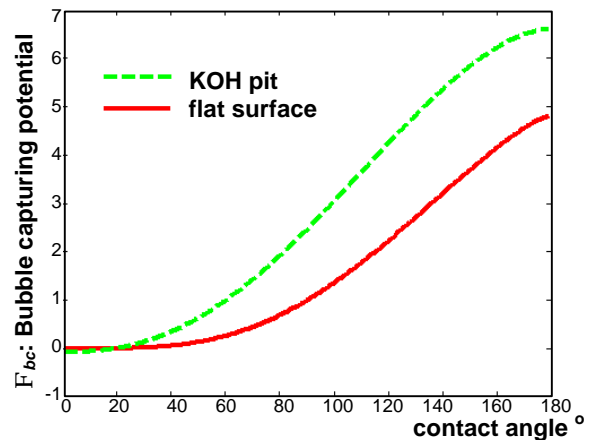
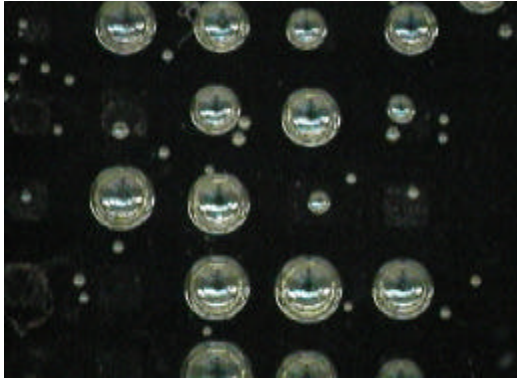


Figure 6. Simulation result of  $F_{bc}$

## EXPERIMENTAL VERIFICATION

In order to verify the bubble capturing concept experimentally, a hydrophilic sample is prepared by thermally growing silicon oxide on a bare silicon wafer (contact angle:  $\theta \sim 20^\circ$ ). HMDS is vapor-coated and patterned by lift-off process to provide relatively hydrophobic spots (contact angle:  $\theta \sim 80^\circ$ ) in a square-grid pattern. The sample is then immersed in 5%  $\text{H}_2\text{SO}_4$  aqueous solution. When hydrogen and oxygen gas bubbles are generated by electrolysis and brought to the sample surface by buoyancy, the gas bubbles preferentially attached to the hydrophobic spots, as figure 7 demonstrates. Around 60% of the flat hydrophobic patterns successfully captured a gas bubble with similar size onto them.



**Figure 7.** Gas bubbles captured on an array of type I bubble-traps

Type II bubble-traps are implemented by paramedic pits etched into a (100) silicon wafer by 30% KOH with  $\text{SiO}_2$  as a mask. The bare silicon, with a contact angle of  $\sim 80^\circ$ , serves as type II bubble-traps (hydrophobic concave pits) on a hydrophilic  $\text{SiO}_2$  surface. Under similar experimental conditions, the KOH-etched pits provide better bubble capturing performance than the HMDS flat pits did, as shown in figure 8. Around 90% of the KOH-etched pits in this experiment successfully captured a gas bubble with similar size onto them.

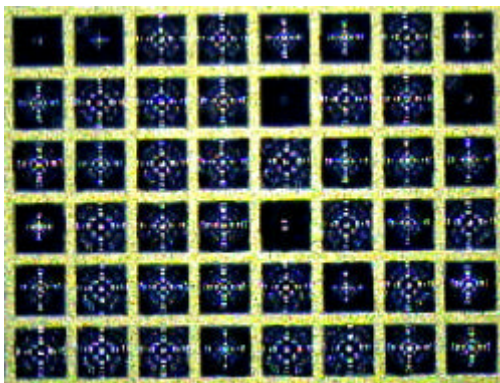


**Figure 8.** Gas bubbles captured on an array of type II bubble-traps

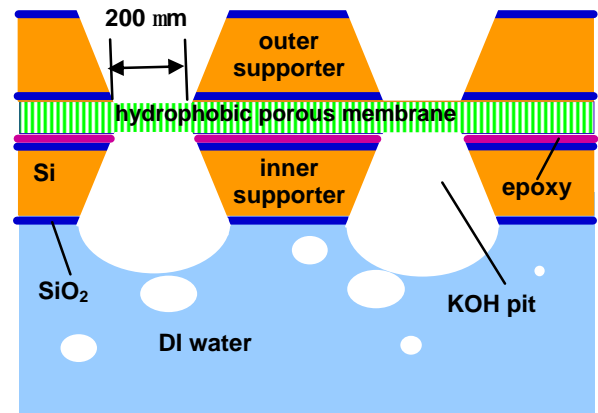
The experiment confirmed that both kinds of bubble-traps can be used to capture bubbles and form bubble arrays. Type II

bubble-traps give better bubble capturing performance, which agrees with the simulation result and supports our proposition to use  $F_{bc}$  as an indicator of the surface's ability to capture bubbles.

## AN APPLICATION: BUBBLE CAPTURING BREATHER

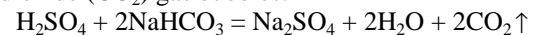
The ability to design bubble-traps on a theoretical foundation with a quantitative measure has led us to design a new gas breather, while there are still many other potential applications for bubble-traps, as stated in the introduction. The breather [8] can be integrated into a microreactor (e.g. micro Direct Methanol Fuel Cell) to remove gas bubbles from the gas/liquid mixture throughout the flow region, rather than at a discrete separator. In this way, the breather can decrease flow resistance, increase the effective reaction area and release chamber pressure. The breather is also designed to collect the gas bubbles from the main flow and capture them to breathing sites on its surface. The rest of the surface area of the microreactor can therefore be saved for other functional structures, such as electrodes or catalyst. Once captured, the bubbles can be breathed out through hydrophobic breathing holes. If the size of breathing holes is small enough (e.g. submicron), the liquid can be held by the surface tension of its own meniscus, while the gas bubbles are breathed out freely.

Figure 9 shows the schematic drawing of a bubble-capturing breather, with a hydrophobic porous membrane [9] sandwiched between two identical KOH-etched silicon chips (type II bubble-traps).



**Figure 9.** Configuration of gas capturing breather with type II bubble traps

Sodium bicarbonate ( $\text{NaHCO}_3$ ) solution and weak sulfuric acid ( $\text{H}_2\text{SO}_4$ ) are sequentially injected into the microchamber by two individual syringes. The chemical reaction generates carbon dioxide ( $\text{CO}_2$ ) gas bubbles:



These  $\text{CO}_2$  gas bubbles are then breathed out through the hydrophobic breathing holes, under proper conditions.

The breathing process was recorded by a CCD camera, as shown in Figure 10: large  $\text{CO}_2$  bubbles shrink into small ones, which can be confined within the KOH-etched pits and will no longer block the flow.

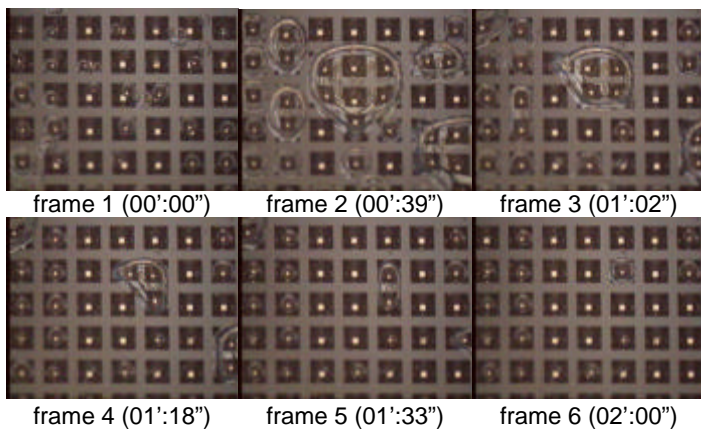


**Figure 10.** Experiment video of a working breather: collect and breathe out gas bubbles

Although the bubble-capturing concept has currently been applied to  $\mu$ -DMFC designs, it provides a new tool for many other applications where ordered micro bubbles on a surface are desired.

## CONCLUSION

Bubble capturing by using surface tension is described in this paper.  $F_{bc}$  is proposed as the quantitative parameter to evaluate a bubble-trap's tendency to capture bubbles. The merit of this definition is that  $F_{bc}$  can be expressed in term of two measurable and controllable variables: surface topology and contact angle  $q$ . Therefore  $F_{bc}$  is independent of the absolute value of surface tension and bubble size, and can be considered as a property of the surface. Simulation of  $F_{bc}$  suggests a distinct performance enhancement for type II bubble-traps (hydrophobic concave pits) over type I bubble-traps (flat hydrophobic patterns), which is confirmed by experiments. Bubble-capturing breather is introduced as an application example.

## ACKNOWLEDGMENTS

This work has been supported by DARPA Micro Power Generation Program. The authors wish to thank Professors C. – M. Ho and X. Zhong, as well as Mr. T. J. Yen, Dr. T.O. Cubaud, Mr. J. Jenkins and Mr. G.J. Shah for their discussion and help.

## REFERENCES

- [1] B. Ran and J. Katz, "The response of microscopic bubbles to sudden changes in the ambient pressure," *Journal of Fluid Mechanics*, vol. 224, (1991).
- [2] A. Akonur and A. K. Prasad, "Methodology and implementation of bubble-image barometry," *Measurement Science and Technology*, vol. 11, (2000).
- [3] M. S. Chawla, X. J. Chen, H. E. Moller, G. P. Cofer, C. T. Wheeler, L. W. Hedlund, and G. A. Johnson, "In vivo magnetic resonance vascular imaging using laser-polarized  $^3\text{He}$  microbubbles," *PNAS*, vol. 95, (1998).
- [4] H. Metcalf, "Sonoluminescence: That Flashing Sound," *Science*, vol. 279, (1998).
- [5] R. P. Taleyarkhan, J. S. Cho, C. D. West, R. T. Lahey, Jr., R. I. Nigmatulin, and R. C. Block, "Additional evidence of nuclear emissions during acoustic cavitation," *Physical Review E (Statistical, Nonlinear, and Soft Matter Physics)*, vol. 69, (2004).
- [6] E. Ostuni, C. S. Chen, D. E. Ingber, and G. M. Whitesides, "Selective Deposition of Proteins and Cells in Arrays of microwells," *Langmuir*, (2001).
- [7] W. Trimmer and R. H. Stroud, "Chapter 2: Scaling of Micromechanical Devices," in *the MEMS handbook*, M. Gad-el-Hak, Ed.: RCR Press, 2002.
- [8] D.-S. Meng, J. Kim, and C.-J. Kim, "A Distributed Gas Breather for the Micro Direct Methanol Fuel Cell," in: *Proceeding of IEEE Int. Conf. Micro Electro Mechanical System (MEMS 2003)*, Kyoto, Japan, (2003).
- [9] D.-S. Meng, T. Cubaud, C.-M. Ho, and C.-J. Kim, "A Membrane Breather for Micro Fuel Cell with High Concentration Methanol," in: *Proceeding of Hilton Head 2004: A Solid State Sensor, Actuator and Microsystems Workshop*, Hilton Head Island, South Carolina, (2004).